UNIVERSITY OF BIRMINGHAM
University of Birmingham Research at Birmingham

The mechanisms governing the activation of dislocation sources in aluminum at different strain rates

Gurrutxaga-Lerma, B.; Balint, D. S.; Dini, D.; Sutton, A. P.

DOI:
10.1016/j.jmps.2015.08.008

License:
Creative Commons: Attribution (CC BY)

Document Version
Publisher's PDF, also known as Version of record

Citation for published version (Harvard):
Gurrutxaga-Lerma, B, Balint, DS, Dini, D & Sutton, AP 2015, 'The mechanisms governing the activation of dislocation sources in aluminum at different strain rates', *Journal of the Mechanics and Physics of Solids*, vol. 84, pp. 273-292. https://doi.org/10.1016/j.jmps.2015.08.008

Link to publication on Research at Birmingham portal

General rights
Unless a licence is specified above, all rights (including copyright and moral rights) in this document are retained by the authors and/or the copyright holders. The express permission of the copyright holder must be obtained for any use of this material other than for purposes permitted by law.

•Users may freely distribute the URL that is used to identify this publication.
•Users may download and/or print one copy of the publication from the University of Birmingham research portal for the purpose of private study or non-commercial research.
•User may use extracts from the document in line with the concept of 'fair dealing' under the Copyright, Designs and Patents Act 1988 (?)
•Users may not further distribute the material nor use it for the purposes of commercial gain.

Where a licence is displayed above, please note the terms and conditions of the licence govern your use of this document.

When citing, please reference the published version.

Take down policy
While the University of Birmingham exercises care and attention in making items available there are rare occasions when an item has been uploaded in error or has been deemed to be commercially or otherwise sensitive.

If you believe that this is the case for this document, please contact UBIRA@lists.bham.ac.uk providing details and we will remove access to the work immediately and investigate.

Download date: 19. Apr. 2024

Journal of the Mechanics and Physics of Solids 84 (2015) 273–292

Contents lists available at ScienceDirect

Journal of the Mechanics and Physics of Solids

journal homepage: www.elsevier.com/locate/jmps

The mechanisms governing the activation of dislocation sources in aluminum at different strain rates

B. Gurrutxaga-Lerma [a,*], D.S. Balint [a], D. Dini [a], A.P. Sutton [b]

[a] Department of Mechanical Engineering, Imperial College London, SW7 2AZ London, UK
[b] Department of Physics, Imperial College London, SW7 2AZ London, UK

ARTICLE INFO

Article history:
Received 4 June 2015
Received in revised form
29 July 2015
Accepted 10 August 2015
Available online 12 August 2015

Keywords:
Frank–Read sources
Homogeneous nucleation
Source activation time
Dislocation dynamics
Yield point

ABSTRACT

This article examines the time to activate Frank–Read sources in response to macroscopic strain rates ranging from $10^1\ s^{-1}$ to $10^{10}\ s^{-1}$ in aluminium under athermal conditions. We develop analytical models of the bowing of a pinned dislocation segment as well as numerical simulations of three dimensional dislocation dynamics. We find that the strain rate has a direct influence on both the activation time and the source strength of Frank–Read sources at strain rates up to $10^6\ s^{-1}$, and the source strength increases in almost direct proportion to the strain rate. This contributes to the increase in the yield stress of materials at these strain rates. Above $10^6\ s^{-1}$, the speed of the bowing segments reaches values that exceed the domain of validity of the linear viscous drag law, and the drag law is modified to account for inertial effects on the motion of the dislocation. As a result the activation times of Frank–Read sources reach a finite limit at strain rates greater than $10^8\ s^{-1}$, suggesting that Frank–Read sources are unable to operate before homogeneous nucleation relaxes elastic stresses at the higher strain rates of shock loading. Elastodynamic calculations are carried out to compare the contributions of Frank–Read sources and homogeneous nucleation of dislocations to plastic relaxation. We find that at strain rates of $5 \times 10^7\ s^{-1}$ homogeneous nucleation becomes the dominant generation mechanism.

© 2015 The Authors. Published by Elsevier Ltd. This is an open access article under the CC BY license (http://creativecommons.org/licenses/by/4.0/).

1. Introduction

The plastic response of metals subjected to loads imposed at different rates varies from the quasi-static response observed in conventional tensile tests (vid. Reed-Hill et al., 2009; Argon, 2008), to one characterised by the formation of shock waves under high strain rate loading (vid. Meyers, 1994; Swegle and Grady, 1985; Grady, 2010). In both regimes, plastic deformation is governed by the kinetics of the generation and motion of dislocations (Hirth and Lothe, 1982). The dominant mechanisms of plastic deformation of the material are those that effect the most rapid relaxation of the imposed elastic stress.

In the quasi-static regime, plastic behaviour is governed by phenomena ranging from thermally activated motion of dislocations during creep and rupture to the plastic yielding of materials subjected to relatively small loads applied at low strain rates where slip is governed by the motion of pre-existing dislocations and by the generation of additional dislocations at Frank–Read sources (Hirth and Lothe, 1982).

* Corresponding author.
E-mail address: benat.gurrutxaga-lerma10@imperial.ac.uk (B. Gurrutxaga-Lerma).

http://dx.doi.org/10.1016/j.jmps.2015.08.008
0022-5096/© 2015 The Authors. Published by Elsevier Ltd. This is an open access article under the CC BY license (http://creativecommons.org/licenses/by/4.0/).

In the shock loading regime, plastic deformation is dominated by the formation of shock waves. Both the propagation speed and the main features of the shock wave profile depend on the intensity of the loading or, equivalently, on the strain rate (vid. Swegle and Grady, 1985; Grady, 2010). For loads up to approximately the shear modulus (Meyers, 1994; Lloyd et al., 2014), there is a dual shock wave front structure, where a faster *elastic precursor* wave propagating at the longitudinal speed of sound precedes a slower *plastic wave* front. Both dislocation activity (Meyers et al., 2009; Murr and Kuhlmann-Wilsdorf, 1978) and twinning (Armstrong et al., 2007; Armstrong and Li, 2015) play a fundamental role under shock loading, although additional effects related to lattice compressions might arise as well (Meyers, 1994). Although dislocation activity is generally acknowledged as a dominant contributor at least at the onset of the plastic front (Meyers, 1994; Armstrong et al., 2007; Armstrong and Walley, 2008; Armstrong and Li, 2015), the generation mechanisms operating in the shock loading regime can be radically different from those in the quasistatic regime. As suggested by Gurrutxaga-Lerma et al. (2015b), homogeneous nucleation of dislocations, which is not seen at low strain rates, can explain many of the characteristics of plastic yielding observed under shock loading.

There are various reasons for this behaviour, a primary factor being the finite time required to activate a Frank–Read source. In this article, we explore the athermal activation time of Frank–Read sources through the development of models which we solve analytically and computationally. Our results support the earlier suggestion in Gurrutxaga-Lerma et al. (2015b) that at higher strain rates Frank–Read sources are too slow with respect to the rise time of the shock front to account for a significant amount of plastic deformation before dislocations are generated by homogeneous nucleation.

Our study is focussed on FCC aluminium. In Section 2 we address the activation of Frank–Read sources at imposed strain rates below $10^6\,s^{-1}$. At these strain rates dislocations may be modelled as Volterra discontinuities in an elastostatic continuum. By employing both analytical models and a three-dimensional model of discrete dislocation dynamics, we explore the effect of increasing the strain rate on the time and critical stress to activate a Frank–Read source. We show that these models start to break down at the higher strain rates, where dislocation speeds are in excess of the range of validity of the assumption that the viscous drag on the dislocation is proportional to its speed. Section 3 explores the time to activate Frank–Read sources at strain rates above $10^6\,s^{-1}$. Analytical models show that the activation time converges to a finite value as the dislocation speed approaches the transverse speed of sound. As a result, it is concluded that at the higher strain rates Frank–Read sources cannot account for all the dislocation generation at the shock front. Section 4 explores the interplay between Frank–Read source activation and homogeneous nucleation. We use the Dynamic Discrete Dislocation Plasticity (D3P) model of plasticity (vid. Gurrutxaga-Lerma et al., 2013) at shock fronts of various rise times, to identify the strain rates above which homogeneous nucleation of dislocations becomes the dominant generation mechanism. Finally, Section 5 summarises our findings.

2. The activation of Frank–Read sources at strain rates below $10^6\,s^{-1}$

The process by which a Frank–Read source operates is well known (vid. Hirth and Lothe, 1982; Hull and Bacon, 2011), and schematically depicted in Fig. 1. Under the influence of an applied shear stress τ resolved on the slip plane in the direction of its Burgers vector, a pinned dislocation segment bows out against the influence of its line tension which tends to keep it straight. The stress required to continue the bowing out increases to a maximum when the radius of curvature of the dislocation line segment is a minimum. This is the critical stress required to operate the source, beyond which a loop is generated and the process begins again. The critical stress is referred to as the 'strength' of the source. In this section we consider the two main characteristics of the process: the stress and the time required to reach the critical condition to operate the source.

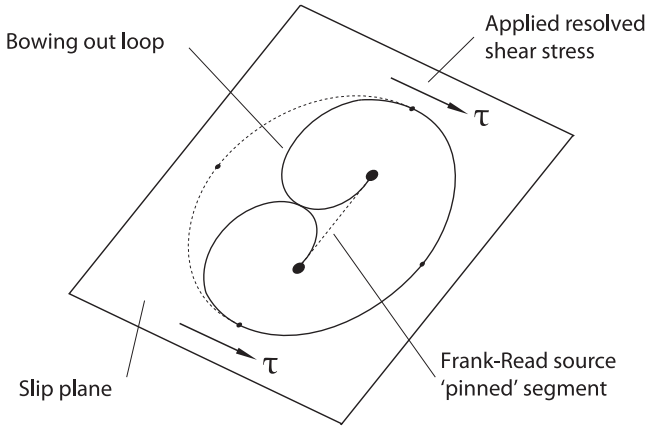

Fig. 1. A Frank–Read source.

2.1. The strength of a Frank–Read source

The strength of a Frank–Read source is the smallest resolved shear stress required to take a pinned dislocation segment to its critical position. The value of this critical stress, τ_{src}, can be understood as a balance between the dislocation line tension, which is the self-stress the dislocation segment acquires as a result of its curvature (Brown, 1964), and the applied resolved shear stress, τ. The effective line tension is a function of the curvature of the dislocation segment (Hirth and Lothe, 1982), and depends logarithmically on the segment length (Brown, 1964; Foreman, 1967). In the following we assume elastic isotropy.

Brown (1964) and Foreman (1967) proposed the source strength to be of the form

$$\tau_{src} = \beta \frac{\mu b}{l_{FR}} \tag{1}$$

where l_{FR} is the segment length, μ the shear modulus, b the magnitude of the Burgers vector and β is defined by Foreman (1967):

$$\beta = \frac{A}{2\pi}\left[\ln \frac{l_{FR}}{r_0} + B\right] \tag{2}$$

where A and B are material constants of order unity, and r_0 is the radius of the dislocation core. The parameter $A=1$ for edge dislocations and $A = 1/(1-\nu)$ for screw dislocations. The parameter B is associated with the nature of the local elastic field (Foreman, 1967). For a source segment of edge character in FCC copper, subjected to a pure shear stress on its slip plane, $A=1$ and $B=0.5$ (Shishvan et al., 2008; Shishvan and Van der Giessen, 2010); for FCC aluminium, following a procedure analogous to that outlined by Shishvan et al. (2008), we estimate that for a source segment of edge character, $A=1$, $B=-3.4$.

The strength of Frank–Read sources directly affects the yield point of a material. Plastic yielding is a process involving both the glide of pre-existing dislocations (Hirth and Lothe, 1982) and the generation of more dislocations. The strength of Frank–Read sources is thus one of the factors controlling the yield stress of a material. If the strength of Frank–Read sources is, on average, $\bar{\tau}_{src}$ and all preferential sources are located in planes at $\pm 45^\circ$ with respect to the direction of the assumed uniaxial loading then the yield point will be reached when the applied stress is $\sigma = 2\cdot\bar{\tau}_{src} \equiv \sigma_{yp}$. Hence, the strength of Frank–Read sources controls the yield point of a crystalline material, at least as long as Frank–Read sources remain the dominant mechanism to generate dislocations.

2.2. Strain rate dependence of the source strength

The source strength τ_{src} in Eq. (1) assumes the dislocation moves at an infinitesimal speed. In practice the dislocation always moves at a finite speed, and that may be expected to increase the source strength owing to the associated dissipation of energy. The speed of the dislocation changes in response to the imposed strain rate.

Consider a Frank–Read source subjected to a local resolved shear stress τ. If $\dot{\epsilon} = d\epsilon/dt$ is a constant imposed uniaxial strain rate the resolved shear stress on planes at 45° to the stress axis increases at the rate $\dot{\tau} = \mu\dot{\epsilon}$. Integrating, it is found that $\tau = \mu\cdot\dot{\epsilon}\cdot t + C$ where C is an integration constant. If we equate this resolved shear stress to the strength of the Frank–Read source then C may be identified with the source strength, τ_0, when the strain rate is zero. Then the source strength τ_{src} at finite strain rates becomes

$$\tau_{src} = \mu\cdot\dot{\epsilon}\cdot t_{nuc} + \tau_0 \tag{3}$$

where $t = t_{nuc}$ is the time for the Frank–Read source to reach the critical condition for its operation at the imposed strain rate $\dot{\epsilon}$. Expressions of this kind can be found in Fan et al. (2012) and Agnihotri (2015). The increase in the source strength at a finite strain rate $\dot{\epsilon}$ is thus determined by the time t_{nuc} to reach the critical condition in the operation of the source.

2.3. Numerical computation of the strain rate dependence of the Frank–Read source strength

The strain rate dependence of the source strength can be calculated numerically using a dislocation dynamics code based on elastostatics in three dimensions. The code we use is ParaDiS (Arsenlis et al., 2007). We consider a pinned edge dislocation segment of length $l_{FR} = 4000\sqrt{2}\,b$ lying on a (111) slip plane in aluminium; $\mu = 28.3$ GPa, $\nu = 0.36$, $b = 2.85$ Å. The dislocation mobility is assumed to follow the usual viscous drag law, $v = (1/d)\tau b$ where v is the dislocation speed, $1/d$ is the mobility and d is the drag coefficient and τb is the Peach–Koehler glide force per unit length of dislocation. We use the mathematical form of drag coefficients defined in Bulatov and Cai (2006), where $d_{edge} = 2\times 10^{-5}$ Pa s for the edge component, and $d_{screw} = 6\times 10^{-5}$ Pa s for the screw components, which were obtained from molecular dynamics simulations of aluminium by Olmsted et al. (2005). The core width is set to one Burgers vector, i.e., $r_c = b$ (Cai et al., 2006). The simulation is carried out with a cubic simulation box of side 35,000 Burgers vectors. The box is subjected to a constant rate of shear strain acting on the (111) plane in the direction of the Burgers vector, ranging from 10 s^{-1} to 10^6 s^{-1}. Following Wang et al. (2007) at any given instant in time, t, the total shear stress is $\tau_{total} = \mu(\dot{\epsilon}t - \epsilon_p)$ where ϵ_p is the plastic shear strain due to the dislocation, i.e., the strain relaxation due to the dislocation loops themselves. The Burgers vector of the dislocation was

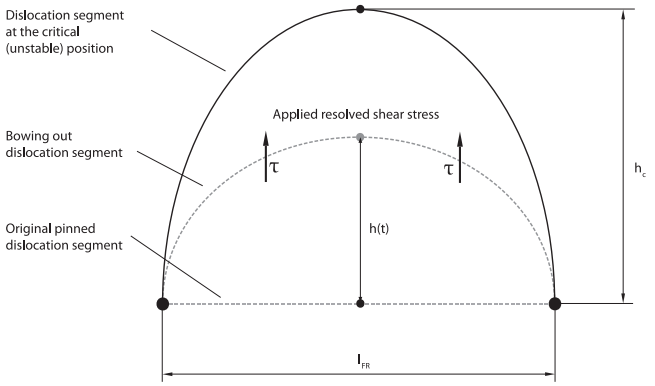

Fig. 2. Schematic of a Frank–Read source segment as it bows out. The critical position h_c is reached when the applied resolved shear stress balances the line tension. Foreman (1967) calculated that for source segments of edge character, this occurs when $h_c \approx 0.75L$, and for source segments of screw character it occurs when $h_c \approx 0.325L$.

$\frac{1}{2}[1\bar{1}0]$. The character of the dislocation was defined as pure edge when its line was along $[11\bar{2}]$, and pure screw when it was along $[1\bar{1}0]$.

2.3.1. *Evolution of the critical configuration with increasing strain rate*

Foreman (1967) argued that for segments of edge character the critical configuration occurs when the centre of the dislocation segment reaches a height of $h_c \approx 0.75l_{FR}$, where l_{FR} is the segment length; for segments of screw character $h_c \approx 0.325l_{FR}$. In our simulations the computed values are smaller than those expected by Foreman's model, but compare well with recent calculations by Shishvan et al. (2008).

Our simulations also show that the critical position is dependent on both the strain rate and the magnitude of the drag coefficients assumed for edge and screw dislocations. This is apparent in Fig. 3, which shows the critical configurations of a

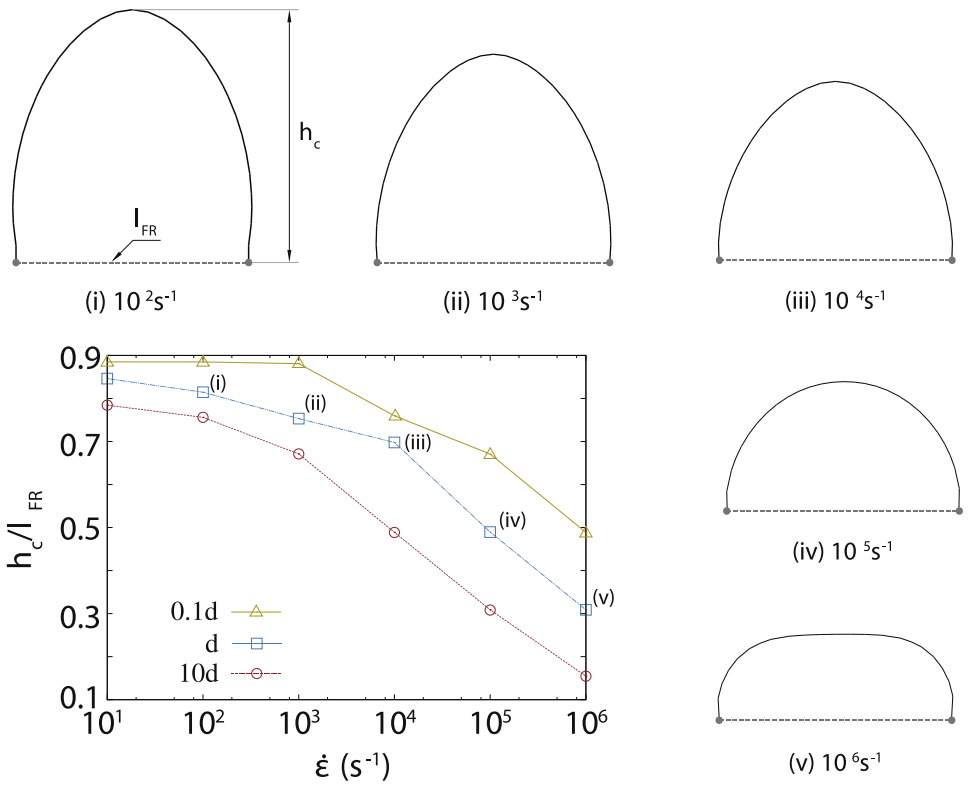

Fig. 3. Computed values of the critical excursion h_c of the Frank–Read source segment relative to its length l_{FR}. d denotes the drag coefficient; $10d$ and $0.1d$ respectively indicate that the drag coefficients of both the edge and screw components were scaled by a factor of 10 and 0.1 throughout the simulations. The shapes of the Frank–Read source segment at the critical configurations for different strain rates are shown in (i) to (v), for the case where the drag coefficients were not scaled. As found by Foreman (1967) the critical segment displays slight bowing to the right and left near the pinning points.

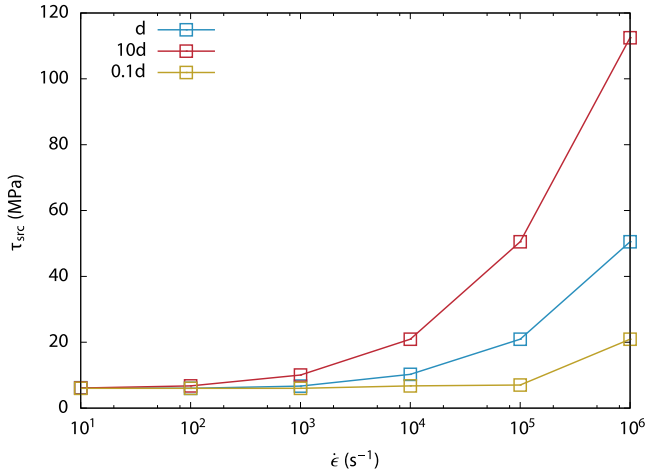

Fig. 4. The critical stress τ_{src} to activate a Frank–Read source as a function of strain rate $\dot{\epsilon}$. The 3 curves refer to the 3 sets of drag coefficients described in Fig. 3. The strain rate is on a logarithmic scale.

Frank–Read source segment, initially of length $l_{FR} = 4000\sqrt{2}\,b$, loaded at different rates. At low strain rates (1–10 s^{-1}), the critical height is about $h_c = 0.85 l_{FR}$ for segments of edge character. The value of h_c decreases with increasing strain rate to about $h_c = 0.3 l_{FR}$ at $\dot{\epsilon} = 10^6$ s^{-1}. This decrease of h_c is accompanied by a noticeable deviation from the 'oval' (Foreman, 1967) or elliptical (Benzerga, 2008) shapes obtained at lower strain rates. For instance, at 10^6 s^{-1}, the critical configuration, shown in Fig. 3(v), has flattened out in the central portion.

The change of shape of the critical configuration stems from the fact that the drag coefficient of edge components is about three times smaller than that of screw dislocations. In a given time step the resolved shear stress is the same on all dislocation segments, but segments with larger edge component travel further than those with larger screw component. This leads to more of the dislocation developing edge character, and therefore the shape of the critical configuration becomes flatter, as seen in Fig. 3.

2.3.2. *Evolution of the source strength with the strain rate*

Fig. 4 shows the strain rate dependence of τ_{src}, calculated according to Eq. (3). Referring to the curve in Fig. 4 labelled by 'd', and noting the logarithmic scale of the strain rate axis, the increase of τ_{src} is almost linear at strain rates up to 10^4 s^{-1}; then, the DD results are fitted reasonably well by

$$\tau_{src} = 6.12 + 4.16 \times 10^{-4}\dot{\epsilon} \text{ MPa} \tag{4}$$

where $\dot{\epsilon}$ is expressed in s^{-1}. However, at higher strain rates the values of τ_{src} deviate significantly from this linear relationship.

According to Eq. (3) the other parameter expected to influence the source strength is the time, t_{nuc}, taken to reach the critical configuration. At strain rates less than 10^4 s^{-1} the DD results obtained for this time are fitted well by

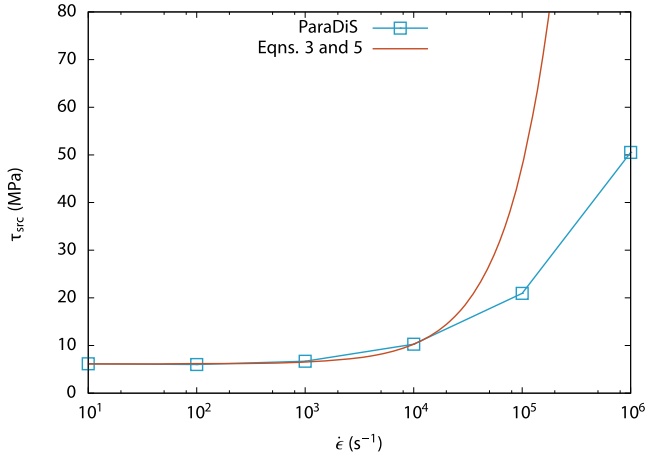

Fig. 5. Deviation between the values of the Frank–Read source strengths obtained at different strain rates by (a) direct simulation using ParaDiS and (b) assuming Eq. (5) holds at all strain rates when it is inserted into Eq. (3). Note the logarithmic scale of the strain rate axis.

$$t_{\mathrm{nuc}} = H + \frac{K}{\dot{\epsilon}} = 1.153 \times 10^{-8} + 2.114 \times 10^{-4} \times \dot{\epsilon}^{-1}(s) \tag{5}$$

where H and K are constants. Notice that in Eq. (5) $t_{\mathrm{nuc}} \to \infty$ in the limit $\dot{\epsilon} \to 0$, which is consistent with no dislocation generation when there is no applied stress.

Combining Eq. (5) with Eq. (3), we obtain

$$\tau_{\mathrm{src}} = (\tau_0 + \mu K) + \mu H \dot{\epsilon} \tag{6}$$

which has the form of Eq. (4), demonstrating that Eqs. (3)–(5) are, within the error of the fit, consistent with each other: $\mu H = 428.12$ Pa ≈ 416 Pa in Eq. (4), and $\tau_0 + \mu K = 5.98$ MPa ≈ 6.12 MPa in Eq. (4).

However, as the strain rate is increased above 10^4 s^{-1} Eq. (5) becomes inaccurate. Fig. 5 shows the deviation between the values of τ_{src} obtained by (a) assuming t_{nuc} is given by Eq. (5) at all strain rates, and (b) the actual values obtained by the ParaDiS simulations. As discussed in the following section the causes of the breakdown of Eq. (5) are related to the change in the shape of the critical configuration, seen in Fig. 3, as the strain rate is increased.

The dramatic increase of the source strength at strain rates above 10^4 s^{-1} can be compared with the increase in the strain rate sensitivity of the yield point, defined as

$$m = \frac{\partial \ln \sigma_{yp}}{\partial \ln \dot{\epsilon}}. \tag{7}$$

As reported by Regazzoni et al. (1987), in many cubic metals including FCC aluminium, HCP zinc, FCC copper and BCC tantalum, the strain rate sensitivity tends to increase an order of magnitude, from $m \approx 0.01$ at strain rates less than 10^3 s^{-1} to $m \approx 0.2$ at strain rates greater than 10^3–10^4 s^{-1}. The calculations performed here on the evolution of τ_{src} allow direct comparison with the strain rate sensitivity of the yield point σ_{yp} of aluminium; this is because the onset of plastic yielding coincides with the activation of Frank–Read sources (Van der Giessen and Needleman, 1995), so even though σ_{yp} and τ_{src} do not share the same quantitative values, it is expected that the strain rate sensitivities of τ_{src} and σ_{yp} will be comparable.

Fig. 6 shows a comparison between the strain rate sensitivity of τ_{src} computed with ParaDiS, and the strain rate sensitivity of the yield point of aluminium obtained from experimental data by Klopp et al. (1985). The strain rate sensitivity of the computed τ_{src} below 10^3 s^{-1} is $m \approx 0.009$, whilst above 10^3 s^{-1}, $m \approx 0.38$. As said, this behaviour agrees reasonably well with the commonly observed values of m for many cubic metals (vid. Follansbee et al., 1984) and with the experimental data obtained by Klopp et al. (1985) for FCC aluminium. It is also noted that, as conventional knowledge holds for FCC metals (see Armstrong and Li, 2015), our model predicts a very small strain rate sensitivity of the source activation strength for strain rates below 10^4 s^{-1}.

It is also interesting to compare our simulations with those of Agnihotri (2015). They used discrete dislocation plasticity (DDP) in which the source strength was assumed to depend on the strain rate, in a manner similar to Eq. (3), and they assumed the activation time of the source depends on the source strength. They found an increase in the yield point with the strain rate which they associated with the strain rate variance of the source strength. The resulting increase in the yield point with strain rate, and the underlying strain rate sensitivity, closely match that computed here for the source strength.

2.3.3. *Evolution of the activation time with the strain rate*

The activation time is the time taken by the source segment to reach the critical position. Benzerga et al. (2004) and Benzerga (2008) calculated the activation time analytically for the quasistatic case, and we follow their procedure here for a

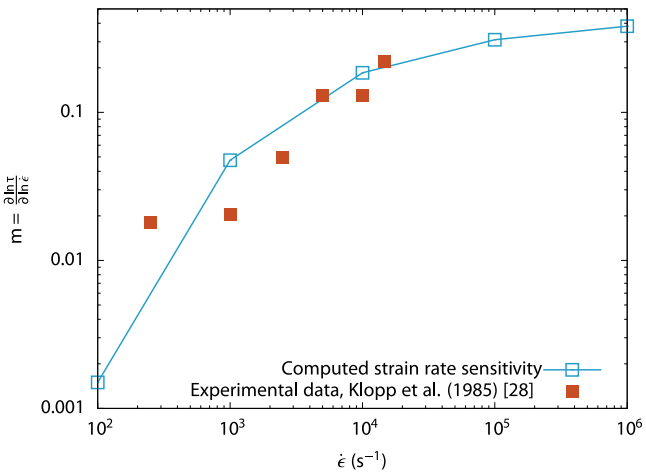

Fig. 6. Strain rate sensitivity as a function of strain rate for the computed stress, τ_{src}, to activate a Frank–Read source, compared with experimental data for the strain rate sensitivity of the yield point in aluminium.

finite strain rate.

Consider a straight source segment of length l_{FR} as depicted in Fig. 2. Let the x-axis be parallel to this straight segment, with $x=0$ at its far left so that the straight segment lies in $0 \le x \le l_{FR}$. The segment bows out as a result of the resolved shear stress τ acting on the slip plane. Its configuration at time t is defined by the perpendicular distance $h(x, t)$ of an element of the bowed loop from the x-axis. Consider the force balance on the central element at $x = l_{FR}/2$ between the Peach–Koehler force, the viscous drag and the line tension:

$$\tau b = d \cdot v(t) + \frac{\mu b^2}{R(t)} \tag{8}$$

where $v(t) = dh(l_{FR}/2, t)/dt$ is the segment velocity and $R(t)$ is the radius of curvature of the central segment. We have approximated the line tension by $\mu b^2/2$. Define $h(l_{FR}/2, t) \equiv h(t)$ for brevity. The radius of curvature $R(t)$ can be estimated by assuming that the bowed segment is the arc of a circle of radius $R(t)$ as follows:

$$R(t) = \frac{h(t)}{2} + \frac{l_{FR}^2}{8h(t)} \tag{9}$$

Substituting this into Eq. (8) yields a separable differential equation, where

$$\frac{\tau b}{d} \int_0^{t_{nuc}} dt = \int_0^{l_{FR}/2} g(h)\, dh \tag{10}$$

in which

$$g(h) = 1 + \frac{\tau_0}{\tau} \frac{h l_{FR}}{h^2 - (\tau_0/\tau) l_{FR} h + (l_{FR}^2/4)}. \tag{11}$$

The activation time can therefore be expressed as

$$t_{nuc} = \frac{1}{2} \frac{l_{FR} d}{\tau b} \mathcal{F}(\xi) \tag{12}$$

with $\xi = \tau/\tau_0$ and

$$\mathcal{F}(\xi) = 1 + \frac{2}{\xi}\left[\frac{1}{2} \ln\left(\frac{2(\xi-1)}{\xi}\right) + \frac{1}{\sqrt{\xi^2-1}} \tan^{-1} \sqrt{\frac{\xi+1}{\xi-1}}\right] \tag{13}$$

This derivation assumes the loop bows into circular arcs. Benzerga (2008) treated the case of elliptical arcs. The underlying physics is the force balance in both cases.

Constant strain rate: Eq. (12) assumes that the applied loading is constant. Here, we consider the effect of a finite, constant strain rate by writing

$$\tau = \tau(t) = \mu \dot{\epsilon} t \tag{14}$$

where $\dot{\epsilon}$ is a constant. The force balance, Eq. (8), becomes

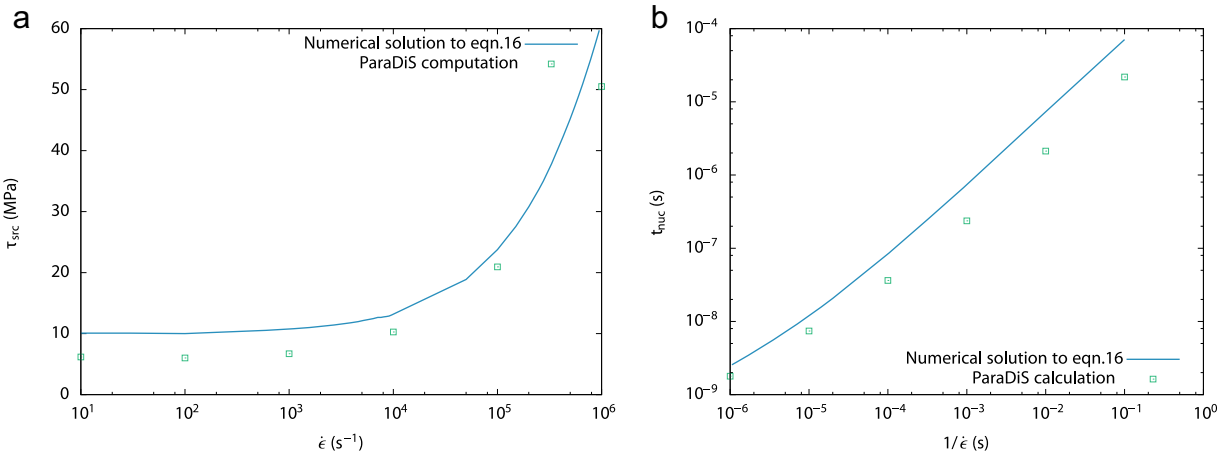

Fig. 7. (a) The Frank–Read source strength as a function of strain rate, and (b) the time to activate the Frank–Read source as a function of the inverse strain rate, obtained by solving Eq. (16) numerically (continuous curves) compared with solutions (discrete points) obtained by ParaDiS simulations. Note the logarithmic scales.

$$\mu\dot{\epsilon}bt = dv(t) + \frac{\mu b^2}{R(t)} \tag{15}$$

which can be rewritten as

$$\frac{dh(t)}{dt} = \frac{1}{d}\left[\mu\dot{\epsilon}bt - \frac{\mu b^2 8h(t)}{4h^2(t) + l_{FR}^2}\right]. \tag{16}$$

An analytic solution has not been found.

Under a monotonically increasing driving force the critical height of the segment continues to be defined by the condition $h(t_{nuc}) \equiv h_c = l_{FR}/2$. This is because irrespective of loading, the radius, $R(t)$, of the bowed segment is a minimum when $h(t) = l_{FR}/2$. When $h(t) > h_c$ the magnitude of the restraining force arising from the line tension is smaller than at the critical configuration, and the applied stress $\tau(t)$ is sufficient to operate the source.

We solved Eq. (16) numerically using a 5th order backward differentiation algorithm (vid. Iserles, 2009). Having obtained $h(t)$ the source activation time, t_{nuc}, was defined by the condition $h(t_{nuc}) = l_{FR}/2$ for a circular arc. The source strength is then given by $\tau_{src} = \tau(t_{nuc}) = \mu\dot{\epsilon}t_{nuc}$. For aluminium, $l_{FR} = 4000\sqrt{2}\,b$ and strain rates between $1\ s^{-1}$ and $10^6\ s^{-1}$, the curves in Figs. 7a and b show the solutions for τ_{src} and t_{nuc} obtained by solving Eq. (16). The points on these figures are the values obtained from ParaDiS simulations, and it is seen that there is reasonable agreement. The overestimation of t_{nuc} and τ_{src} by the analytical model is presumably related to the assumption that the bowed dislocation is an arc of a circle. In the ParaDiS simulations no such assumption is made, and the dislocation segment may assume an oval shape, as seen in Fig. 3, which varies with the strain rate. The results of the ParaDiS simulations are closest to the analytical results when $\dot{\epsilon} \approx 10^5\ s^{-1}$. At this strain rate the critical configuration, shown in Fig. 3(iv), is closest to being a semi-circle.

There is a rapid increase in the source strength, τ_{src}, as seen in Fig. 7, that begins at strain rates between 10^3 and $10^4\ s^{-1}$. At strain rates up to $10^3\ s^{-1}$ the very slight increase in the source strength with strain rate is consistent with Eqs. (3)–(5). Since the source strength satisfies Eq. (3) at all strain rates the steep increase of τ_{src} indicates that the product $\dot{\epsilon}t_{nuc}$ increases rapidly with strain rate. This is consistent with the positive deviation from the linear relationship between t_{nuc} and $1/\dot{\epsilon}$ seen in Figs. 7 and 8 at strain rates above $10^3\ s^{-1}$ for the standard drag coefficients. Fig. 8 provides evidence that the deviation is directly related to the drag coefficients because it is seen that the onset of the deviation can be controlled by altering the drag coefficients. That is, the onset of the deviation occurs at a lower (higher) strain rate if the drag coefficients are increased (decreased).

2.4. Upper bound on the strain rate for the validity of the previous models

The dislocation dynamics simulations and the analytical treatments of previous sections are limited to strain rates where inertial effects in the motion of dislocations may be ignored. This is because the dislocation speed may exceed the limit for which the assumed linear viscous drag law is valid. In that case neither the drag law nor the elastic fields of the dislocations can be treated quasistatically, and an elastodynamic treatment is required.

Molecular dynamics simulations of edge dislocation motion (Olmsted et al., 2005) in aluminium suggest that the linear viscous drag model breaks down when the dislocation speed exceeds 1000 m/s. In the ParaDiS simulations of the previous

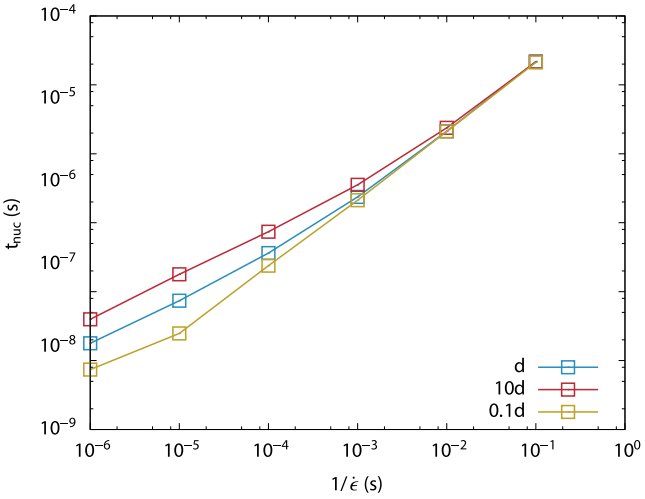

Fig. 8. The activation time of a Frank–Read source plotted against the log of the inverse strain rate for three sets of drag coefficients. At strain rates up to $10^3\ s^{-1}$ the activation time for the standard drag coefficients (i.e. the curve labelled *d*) varies linearly with the inverse strain rate, as in Eq. (5). But at strain rates greater than $10^3\ s^{-1}$ the activation time deviates from this linear relationship and is significantly larger than it predicts. The deviation from this linear relationship begins at smaller (larger) strain rates when the standard drag coefficients are multiplied by 10 (0.1).

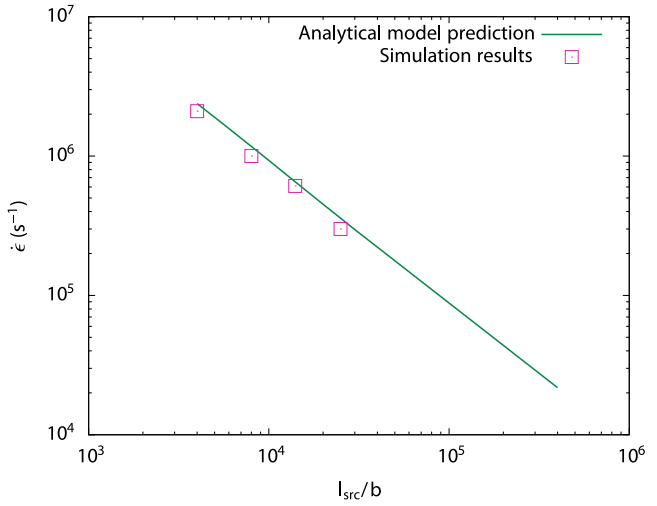

Fig. 9. Limiting strain rates vs length of the Frank–Read source segment, above which inertial effects in dislocation motion become significant.

section, the speed of the dislocation segment surpasses 1000 m/s when the source strength reaches $\tau_{src} \approx 70$ MPa. For $l_{FR} = 4000\sqrt{2}\,b$, this occurs at $\dot{\epsilon} \approx 2 \times 10^6\ s^{-1}$. The analytical model of the previous section predicts the limiting speed to be achieved at about $\dot{\epsilon} = 2.4 \times 10^6\ s^{-1}$. Fig. 9 shows the limiting strain rates for Frank–Read source segments of different lengths, where in all cases the limit is defined by the dislocation speed exceeding 1000 m/s. The data in this figure are fitted by

$$\dot{\epsilon}_{limit} = \frac{9.44 \times 10^{10}}{l_{FR}/b} s^{-1}. \tag{17}$$

The limiting strain rate is inversely proportional to the length of the Frank–Read source segment. In a real material, this length is a random variable that follows a log-normal distribution (Shishvan and Van der Giessen, 2010), and is bounded by the grain size; for typical grain sizes of the order of a few microns, one can estimate a source length of at most the same order of magnitude (i.e., $l_{FR}/b \approx 10^4$), which according to Eq. (17) entails a limiting strain rate of between 10^6 and $10^7\ s^{-1}$.

Hence, the data presented in Fig. 9 suggests that the validity of an elastostatic, linear viscous drag treatment is doubtful when the strain rate exceeds $10^6\ s^{-1}$ for all but the smallest Frank–Read source segments. The next section presents a more reliable treatment.

3. Frank–Read sources at higher strain rates

There are two principal assumptions in the derivation of the source activation times in Section 2.3.3: (i) a linear viscous drag law can be used for the drag force in the force balance with the line tension and the applied stress, and (ii) the line tension (see Eq. (1)) arises as a result of the increase in the *elastostatic* energy of the dislocation when it acquires curvature.

As explained in Section 2.4, the validity of the linear viscous drag law is limited to dislocation speeds of less than about 1000 m/s in aluminium, which corresponds to a strain rate $\dot{\epsilon} \approx 10^6\ s^{-1}$.This section examines the case where the speed of the dislocation segment exceeds this limit.

3.1. Drag laws

The drag law plays a fundamental role in determining the dynamics of the activation of Frank–Read sources. For dislocations moving at small speeds compared to the transverse wave speed, the increase in the self-energy of the dislocation as a result of the dislocation motion is negligible. However, when the dislocation speed becomes a significant fraction of the transverse speed of sound, typically $\gtrsim 0.4c_t$, the increase in the self-energy of the dislocation is sometimes accounted for by an *inertial* force, and the dislocation is imbued with an effective mass (Meyers, 1994; Weertman, 1961; Hirth et al., 1998; Ni and Markenscoff, 2008; Gurrutxaga-Lerma et al., 2014):

$$f_{inertia} = m\frac{dv_{glide}}{dt}$$

where m is the effective mass per unit length of the dislocation.

The exact form of m or $f_{inertia}$ depends on the kinematic state of the dislocation. A uniformly moving dislocation cannot increase its elastic self-energy, so the forms of m found in Meyers (1994), Weertman (1961), and Hirth et al. (1998) must be

regarded as approximations at best. A proper treatment of inertia treats the elastodynamic self-energy explicitly. Clifton and Markenscoff (1981), employing previous elastodynamic solutions to the fields of a dislocation (Markenscoff, 1980; Markenscoff and Clifton, 1981), reached an expression for the inertial effects for the case of straight edge and screw dislocations with a non-regularised core. In general, the motion of a dislocation is expected to be non-uniform. For screw dislocations, a rigorous treatment of inertia can be found in Ni and Markenscoff (2008), where an expression of the dislocation effective mass for regularised dislocation cores can be found. For edge dislocations, Pellegrini (2014) has provided a complete treatment of dislocation drag including inertial effects based on a regularised core, using a dynamic Peierls–Nabarro model. Previously, Pillon et al. (2007), again within the Peierls–Nabarro framework, provided an approximate equation of motion for edge and screw components that accounted for retardation effects.

Experimental evidence (Johnston and Gilman, 1959; Nix and Menezes, 1971) and atomistic simulations (Olmsted et al., 2005; Koizumi et al., 2002; Tsuzuki et al., 2008; Bitzek and Gumbsch, 2004, 2005) indicate that inertial effects do limit dislocation speeds. The limit is commonly identified with the transverse speed of sound (Hirth and Lothe, 1982), while for edge dislocations it is sometimes identified with the Rayleigh wave speed (Weertman, 1961; Brock, 1982). The existence of an upper limit implies than an increment in the dislocation speed requires an infinite increment in applied stress. When inertial effects are significant the use of a linear viscous drag law underestimates the activation time of a Frank–Read source.

3.2. Approximate modelling of bowing dislocation segments under large stresses

Several more empirical ways have been proposed to treat the drag of a dislocation segment moving at high speed. One is to modify the drag coefficient, as suggested by Taylor (1969):

$$d = \frac{d_0}{1 - v^2/c_t^2}. \tag{18}$$

For this relationship the drag force, $f_{\text{drag}} = d \cdot v$, becomes infinite as the dislocation speed approaches c_t.

When the Taylor drag coefficient is used in Eq. (8), a non-linear differential equation results

$$\tau b = \frac{d_0}{1 - \frac{1}{c_t^2}\left(\frac{dh}{dt}\right)^2}\frac{dh}{dt} + \frac{\mu b^2}{\frac{h(t)}{2} + \frac{l_{\text{FR}}^2}{8h(t)}} \tag{19}$$

Alternatively, Eq. (8) could be modified by introducing an inertial force. The force balance then becomes

$$m\frac{d^2h}{dt^2} + d_0\frac{dh}{dt} + \frac{\mu b^2}{R(t)} = \tau b \tag{20}$$

where $R(t) = \frac{h(t)}{2} + \frac{l_{\text{FR}}^2}{8h(t)}$ as before. Notice that both in Eqs. (19) and (20) the applied stress, τ, can be time-dependent, e.g. $\tau = \mu\dot{\epsilon}t$ for a constant strain rate. Eqs. (19) and (20) are non–linear differential equations. We consider simple cases for which solutions are available.

3.2.1. Large constant applied stress

When the applied stress τ is much larger than the maximum restraining force arising from the line tension, $\tau \hat{a}^a\text{¢}\, 2\mu b^2/l_{\text{FR}}$, Eqs. (19) and (20) may be simplified as follows:

$$\tau b = \frac{d_0}{1 - \frac{1}{c_t^2}\left(\frac{dh}{dt}\right)^2}\frac{dh}{dt} \tag{21}$$

and

$$m\frac{d^2h}{dt^2} + d_0\frac{dh}{dt} = \tau b. \tag{22}$$

Saturated drag with no inertia: The solution of Eq. (21), with the initial condition $h(0) = 0$ is

$$h(t) = t \cdot \frac{c_t}{2}\left[\sqrt{\left(\frac{c_t d_0}{\tau b}\right)^2 + 4} - \frac{c_t d_0}{\tau b}\right]. \tag{23}$$

Since the activation time of the source is defined by the condition $h(t_{\text{nuc}}) = l_{\text{FR}}/2$, we obtain

$$t_{\text{nuc}} = \frac{l_{\text{FR}}}{c_t\left[\sqrt{\left(\frac{c_t d_0}{\tau b}\right)^2 + 4} - \frac{c_t d_0}{\tau b}\right]} \tag{24}$$

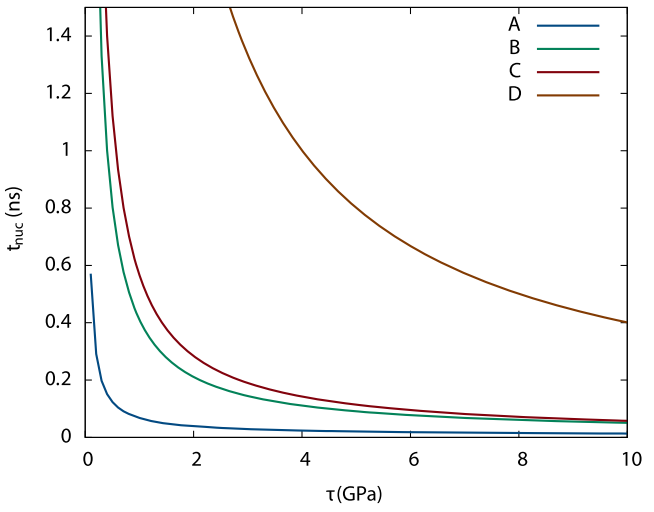

Fig. 10. The source activation time t_{nuc} plotted against the applied stress τ obtained by solving the implicit equation (26) for different values of the drag coefficient d_0 and segment lengths l_{FR}. Here A refers to $l_{FR} = 4000\sqrt{2}\,b$, $d_0 = 2\times10^{-5}$ Pa s; B to $l_{FR} = 4000\sqrt{2}\,b$, $d_0 = 2\times10^{-4}$ Pa s; C to $l_{FR} = 40,000\sqrt{2}\,b$, $d_0 = 2\times10^{-5}$ Pa s; D refers to $l_{FR} = 40,000\sqrt{2}\,b$, $d_0 = 2\times10^{-4}$ Pa s.

For $l_{FR} = 10^{-7}$ m, corresponding to a source strength τ_0 of about 70 MPa, $\tau = 1$ GPa, $d_0 = 10^{-5}$ Pa s, $b = 2.85$ Å, $c_t = 3200$ m/s, we find $t_{nuc} \approx 20$ ps.

Constant drag with inertia: Solving Eq. (22) with the initial conditions $h = 0$ and $dh/dt = 0$ at $t = 0$ we obtain

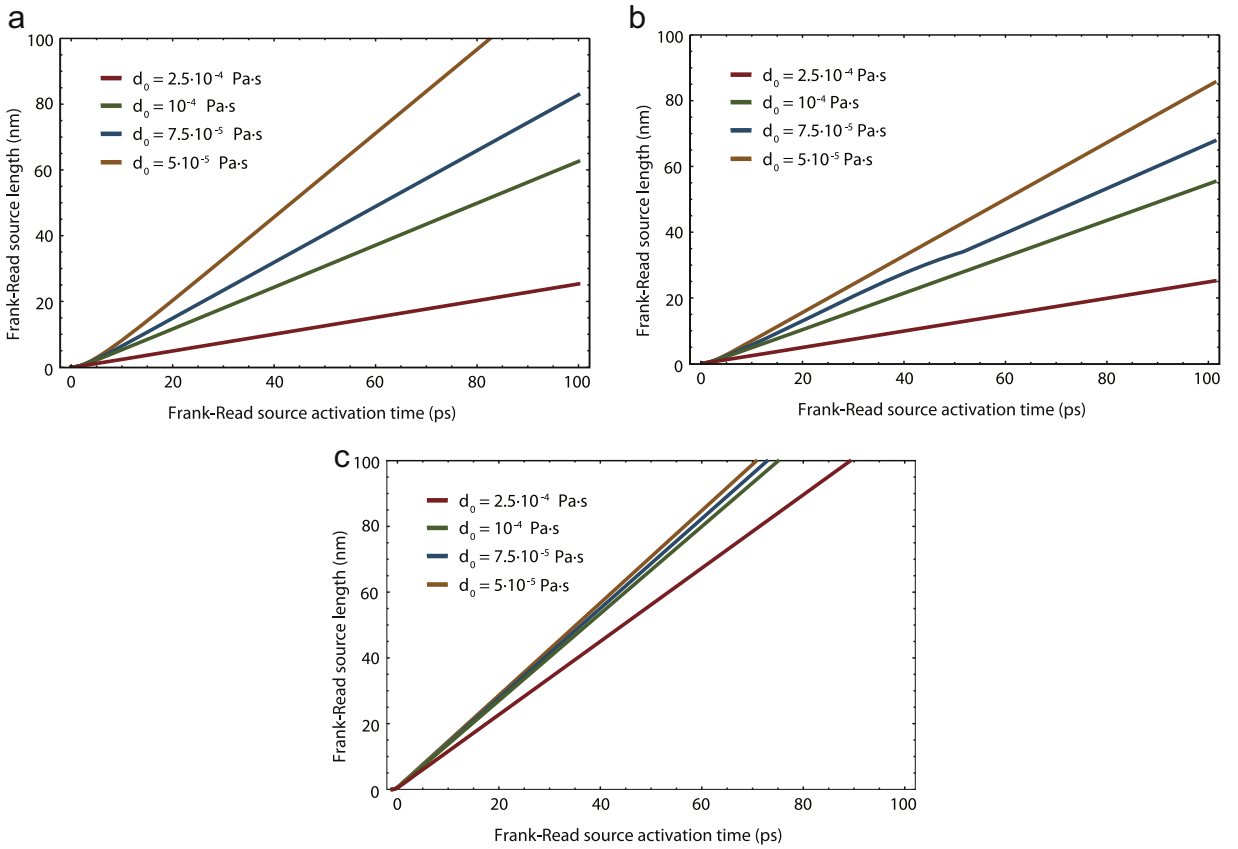

Fig. 11. Numerical solution to Eq. (22) using different definitions of drag and effective mass. (a) $\tau = 2$ GPa, constant drag d_0, effective mass as given in Eq. (27). (b) $\tau = 2$ GPa, velocity-dependent drag (Eq. (18), d_0 as defined in the figure), no effective mass. (c) $\tau = 5$ GPa, constant drag, effective mass as given in Eq. (27).

$$h(t) = \frac{b\tau}{d_0}\left[t - \frac{m}{d_0}\left(1 - e^{-td_0/m} \right) \right], \tag{25}$$

where we have assumed that the effective mass m per unit length is constant. Defining the source activation time by the same condition $h(t_{\text{nuc}}) = l_{\text{FR}}/2$ we obtain an implicit equation for t_{nuc}:

$$t_{\text{nuc}} + \frac{m}{d_0} e^{-t_{\text{nuc}} d_0/m} = \frac{d_0^2 l_{\text{FR}} + 2bm\tau}{2b\tau d_0}. \tag{26}$$

For the same parameter values given above and $m = \rho b^2$ with $\rho = 2700$ kg/m^3, we find $t_{\text{nuc}} \approx 20$ ps.

Fig. 10 shows the variation of source activation times with the applied stress τ and the drag d_0. As expected, the larger the drag, or the larger the segment length, the greater the activation time of the source. However, these values must be considered with some care, as the effective mass is dependent on the dislocation speed.

When a dislocation moves at constant speed it should not experience inertial forces. Nevertheless, the inertial masses proposed by Weertman and Weertman (1980) and Hirth et al. (1998) for uniformly moving pre-existing dislocations capture to some extent the change in elastic self-energy of a dislocation when it moves at different constant speeds. Several expressions of dislocation mass can be found in Weertman and Weertman (1980). For simplicity we use the following:

$$m = \frac{m_0}{\sqrt{1 - \dfrac{v^2}{c_t^2}}} \tag{27}$$

where $m_0 \equiv \rho b^2$. This expression of inertial mass is the first term of an expansion of the inertial mass derived by Weertman and Weertman (1980) for uniformly moving screw and edge dislocations.

By combining Eq. (27) with Eq. (22), the following governing equation is obtained:

$$\frac{m_0}{\sqrt{1 - \dfrac{(dh/dt)^2}{c_t^2}}} \frac{d^2h}{dt^2} + d_0 \frac{dh}{dt} = \tau \cdot b. \tag{28}$$

As before, the source activation time is obtained by equating $h(t_{\text{nuc}})$ to $l_{\text{FR}}/2$. The numerical solution is shown in Fig. 11 for the cases when the segment is loaded with $\tau = 2$ GPa and $\tau = 5$ GPa and for linear viscous drag coefficient d_0, ranging from 5×10^{-5} Pa s to 2.5×10^{-4} Pa s. The activation time is directly proportional to l_{FR}, and inversely proportional to the applied stress τ. Above $\tau \approx 5$ GPa, the curves become virtually insensitive to further increases in τ, suggesting that a limit in the drag has been reached by then; this is in fact in agreement with the behaviour expected from Eq. (26), which for the material parameters chosen here suggests that by 4 GPa the dislocations have reached about 95% of their limiting speed. In either case, these curves display a behaviour that agrees qualitatively with the previous model of constant drag and inertia. As can be appreciated, the activation times in this model often range well above 10–20 ps, obtained in the previous section. For the typical values of aluminium given above we see that, depending on d_0 and the length of the Frank–Read source segment, the activation times can easily exceed 100 ps.

Following Section 3.1, were one to consider in this case a model where both the drag coefficient and the effective mass

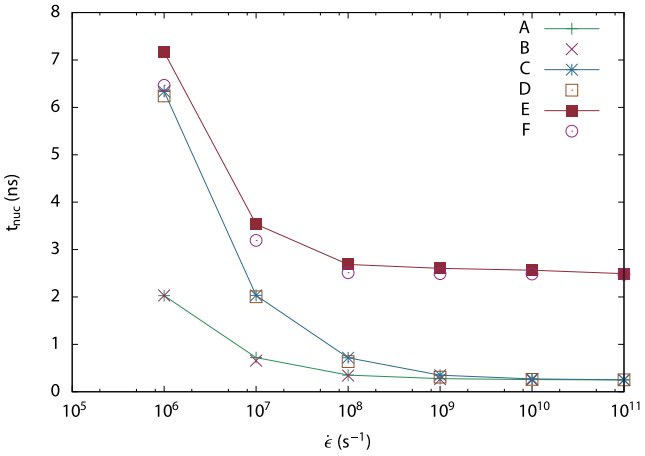

Fig. 12. The source activation times at higher strain rates. The activation times in cases A, C and E, shown as continuous lines, are obtained by numerically solving Eq. (29) for the time when $h(t) = l_{\text{FR}}/2$; for A, $l_{\text{FR}} = 4000\sqrt{2}\,b$, $d_0 = 2 \times 10^{-5}$ Pa s; for C, $l_{\text{FR}} = 4000\sqrt{2}\,b$, $d_0 = 2 \times 10^{-4}$ Pa s; for E, $l_{\text{FR}} = 40,000\sqrt{2}\,b$, $d_0 = 2 \times 10^{-5}$ Pa s. Points labelled B, D and F were obtained with the same input parameters as A, C and E respectively, but the inertial mass equation (Eq. (28)) was solved instead. The agreement between the solutions of the equations is evident.

diverge at c_t, the activation times would become greater still. The numerical solution to this model is also shown in Fig. 11 with dashed lines for $\tau = 2$ GPa. The behaviour displayed there is largely reminiscent of the constant drag coefficient case. As expected, however, activation times are invariably greater than in the previous case, and for source lengths of 10^{-7} m the most conservative estimation places them in the range of 80–100 ps, and most likely well in excess of that. Again, above ≈ 5 GPa the curve was seen to become insensitive to further increases in τ. The activation times are at best in the range of 80–100 ps, so they can be deemed so slow that, when the activation time is compared with the rise time of a shock front ($t_{\text{rise}} \propto 1/\dot{\epsilon}$, so $t_{\text{rise}} = 100$ ps for 10^{10}s^{-1}), further studies of Frank–Read activation at higher stresses seem unnecessary.

3.2.2. Constant strain rate

In this section Eqs. (19) and (28) are solved for a constant strain rate, so that the applied stress increases linearly in time $\tau = \mu\dot{\epsilon}t$.

Eq. (19) may be solved analytically, assuming $\tau \hat{a}^{a}\mathcal{C}\, 2\mu b^2/l_{\text{FR}}$. The solution is

$$h(t) = \frac{c_t^2 d_0}{2\dot{\epsilon} b\mu}\left[\ln\left(\frac{2c_t d_0}{c_t d_0 + \sqrt{c_t^2 d_0^2 + 4\dot{\epsilon}^2 b^2 \mu^2 t^2}}\right) + \frac{1}{c_t d_0}\sqrt{c_t^2 d_0^2 + 4\dot{\epsilon}^2 b^2 \mu^2 t^2} - 1\right]. \tag{29}$$

Equating $h(t) = l_{\text{FR}}/2$, one can find the activation times t_{nuc}. Eq. (29) defines t as an implicit function of h, which we solve numerically in Fig. 12 to find t_{nuc} for $h = l_{\text{FR}}/2$. The same values of the parameters for aluminium as before have been used. Two segment lengths have been considered, $l_{\text{FR}} = 4000\sqrt{2}\,b$ and $l_{\text{FR}} = 40,000\sqrt{2}\,b$, both with $d_0 = 2 \times 10^{-5}$ Pa s. For the segment length $l_{\text{FR}} = 4000\sqrt{2}\,b$ the activation times converge to 250 ps at strain rates above $10^9\ \text{s}^{-1}$ for both $d_0 = 2 \times 10^{-5}$ Pa s and $d_0 = 2 \times 10^{-4}$ Pa s. For the segment of longer length, the behaviour is similar but the activation time converges to about 2.5 ns at a strain rate of about $10^8\ \text{s}^{-1}$.

The levelling off of the activation time with increasing strain rate implies that the segment speed reaches a limiting value. This may be confirmed by differentiating Eq. (29) to get the segment speed:

$$\frac{dh(t)}{dt} = \frac{2bc_t\dot{\epsilon}\mu t}{\sqrt{4b^2\dot{\epsilon}^2\mu^2 t^2 + c_t^2 d_0^2} + c_t d_0} \tag{30}$$

Taking the limit that the strain rate tends to infinity we find

$$\lim_{\dot{\epsilon}\to\infty} \frac{dh(t)}{dt} = c_t, \tag{31}$$

as expected. For $\dot{\epsilon} \approx 10^8\ \text{s}^{-1}$ a segment of length $l_{\text{FR}} = 4000\sqrt{2}\,b$ achieves a limiting speed of about $0.985c_t$, so larger strain rates will change the limiting speed of the segment only very slightly. Since the segment speed is inversely proportional to the activation time, i.e. the time it takes for the centre of the segment to move a distance $l_{\text{FR}}/2$, the activation time and segment speed level off at the same strain rate.

As can be seen in Fig. 12, the numerical solution to the model with a divergent effective mass, defined by Eq. (28), for a constant strain rate, renders very similar results to those provided by Eq. (19) with a divergent drag coefficient. As the strain rate increases the activation time tends to the same limiting values with the two methods, because both approaches lead to the same limiting dislocation speed.

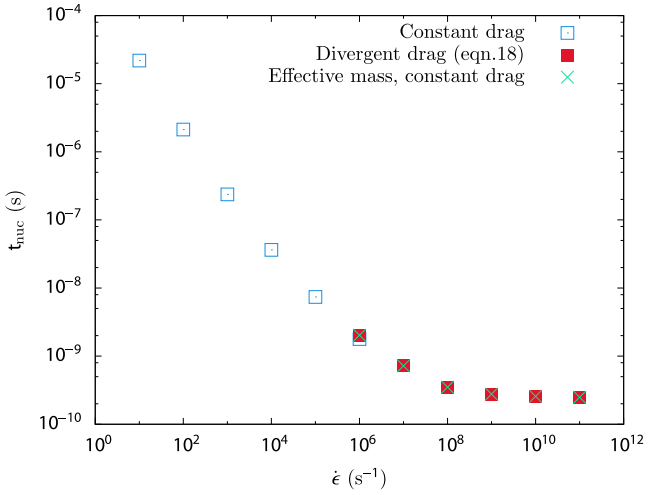

Fig. 13. The Frank–Read source activation time across the whole range of strain rates considered in this article, as predicted by the analytical models.

3.2.3. Discussion

Our results indicate that, even for large applied stresses and strain rates, the activation times of Frank–Read sources are at least of the order of tens of picoseconds. The quasistatic analyses performed in Section 2 employing both analytical and computational dislocation dynamics provide a lower bound to those presented in this section, because they neglect inertial effects which limit the dislocation speed to the transverse speed of sound. If the inertia term is removed from Eq. (20) and it is integrated to calculate t_{nuc} when $h = l_{\mathrm{FR}}/2$, it is found that

$$t_{\mathrm{nuc}} = \frac{l_{\mathrm{FR}}}{2\tau b} d_0 \tag{32}$$

Substituting the typical values of $l_{\mathrm{FR}} = 4000\sqrt{2}\,b$, $\tau = 2$ GPa, and $d_0 = 2 \times 10^{-5}$ Pa s, then $t_{\mathrm{nuc}} \approx 28$ ps. For the same dislocation length, the constant load model of Section 3.2.1 gives an activation time of $t_{\mathrm{nuc}} = 39$ ps. This is comparable to the values obtained in the simulations in Sections 2.3 and 2.3.3. Fig. 13 shows a comparison of the linear viscous drag model and the inertial models considered in this section, displaying the agreement in the trend, and the limiting behaviour of t_{nuc} as the segment speed approaches the transverse speed of sound.

For the dislocation segment length of $4000\sqrt{2}\,b$ the limiting value of the activation time at high strain rates is about 250 ps. For the larger segment length of $40,000\sqrt{2}\,b$, the limiting activation time is about 2500 ps. The rise time is approximately the inverse of the strain rate $t_{\mathrm{rise}} \approx 1/\dot{\epsilon}$. For sources with the shorter segment lengths we deduce that for strain rates above $10^8\ \mathrm{s}^{-1}$ the number of dislocations generated by each source as the shock front passes through is less than 100. With a typical source density of $100\ \mu\mathrm{m}^{-2}$, each producing less than 100 dislocations, the Frank–Read sources will not be able to account for all the 10^4 dislocations per $\mu\mathrm{m}^{-2}$ observed in a shocked sample (Meyers, 1994). This suggests that some other generation mechanism must be operating at strain rates in excess of $10^8\ \mathrm{s}^{-1}$ to account for the dislocation densities observed.

4. Dislocation sources at strain rates up to $10^{10}\ \mathrm{s}^{-1}$

In Section 3, it was shown that at strain rates less than $10^6\ \mathrm{s}^{-1}$ the activation time of Frank–Read sources decreases almost in inverse proportion to the strain rate. It was also shown that for larger strain rates, particularly above $10^8\ \mathrm{s}^{-1}$, the activation time reaches a limiting value and generation rates are insufficient to explain the observed dislocation densities. Alternative dislocation generation mechanisms must be invoked to account for the observed dislocation densities at these higher strain rates.

4.1. Alternative mechanisms for the generation of dislocations at high strain rates

4.1.1. Alternative mechanisms for generation of dislocations

Dislocation multiplication via cross-slip has long been considered an important source of dislocations at relatively high strain rates (vid. Gilman, 1969). Wang et al. (2007) have examined the importance of this mechanism in metallic single crystals subjected to strain rates below $10^7\ \mathrm{s}^{-1}$, finding that it becomes a dominant player in plastic deformation at higher strain rates. However, cross slip might be too slow when the strain rate exceeds $10^8\ \mathrm{s}^{-1}$. Experimental studies of post-shock dislocation structures in FCC materials shocked at strain rates less than $\approx 10^7\ \mathrm{s}^{-1}$ are characterised by the presence of Kuhlmann-Wilsdorf cell patterning (Murr and Kuhlmann-Wilsdorf, 1978), which is consistent with a large degree of cross-slip. However, at strain rates greater than 10^7–$10^8\ \mathrm{s}^{-1}$ the cell patterning is much weaker (Murr, 1988); this suggests that, at sufficiently high strain rate, the time scales required for cross-slip to activate become too large to account for the dislocation generation.

Additionally, heterogeneous nucleation of dislocations at particles, precipitates, grain boundaries or free surfaces may play an important role as the strain rate increases in polycrystalline materials and alloys (see Austin and McDowell, 2011, 2012). Furthermore, the formation of twins is known to play a dominant role in the high strain response of HCP materials (see Price, 1963; Huang and Gray, 1989; Armstrong and Li, 2015).

4.1.2. Homogeneous nucleation

This involves the slip of a localised region of a slip plane to create a dislocation loop, which subsequently expands rapidly under the influence of a large applied stress. The dislocation loop has often been considered to be created with its full Burgers vector from the moment it comes into being, vid. Davis and Hirth (1966) and Hirth and Lothe (1982). The stress required to prevent the immediate collapse of such a loop is so high it has led some to conclude that '*the stress required for homogeneous nucleation [is] three to four times as high as that existing in a highly shocked material*' (Zaretsky, 1995). Nevertheless, the possibility of homogeneous nucleation under high strain rate shock loading was considered a serious contender by Meyers (1978), and also by Weertman and Follansbee (1988), Weertman (1986), amongst others.

Recently, a new process called 'non-local homogeneous nucleation' has been proposed (Gutkin and Ovidko, 2006, 2008). In this mechanism homogeneous nucleation occurs in a nano-scale region of a slip plane where the amount of slip grows in time to the final Burgers vector. Thus, the Burgers vector of the loop increases in time from zero to its final crystallographic

value. A recent analysis by Aubry et al. (2011) provides support for this mechanism in aluminium and nickel, suggesting homogeneous nucleation occurs at stresses of the order of a GPa. This model also appears to resemble what is observed in large-scale MD simulations of shock loading (vid. Bringa et al., 2005, 2006), where nano-loops are seen to form suddenly and collapse or grow. Tschopp and McDowell (2008) have reported similar mechanisms, and shown that homogeneous nucleation is achievable at stresses below the theoretical strength through thermally assisted processes.

4.2. Dynamic discrete dislocation plasticity simulations of source activation at high strain rates

A simple calculation can estimate the range of strain rates where alternative dislocation generation mechanisms are more likely than Frank–Read sources (vid. Malygin et al., 2013). In the absence of any thermal assistance homogeneous nucleation can occur only if the applied stress is at least as large as the theoretical shear strength of the crystal lattice (Tschopp and McDowell, 2008). In shock loading, the peak normal stress σ and the strain rate $\dot{\epsilon}$ are related by the fourth power law (Swegle and Grady, 1985), an empirical relation that holds for almost all materials known, according to which

$$\dot{\epsilon} \propto \sigma^4 \tag{33}$$

A convincing explanation for the universality of this relationship has not appeared, although it has been associated with various dissipative mechanisms at the shock front, including dislocation activity in crystalline materials (Grady, 2010). Recent experimental data (Crowhurst et al., 2011) for strain rates between $10^5\ s^{-1}$ and $10^{10}\ s^{-1}$ has confirmed the fourth power law applies in aluminium. The data in Crowhurst et al. (2011) is fitted by

$$\dot{\epsilon} = 8255.34 \times \sigma^{3.96}, \tag{34}$$

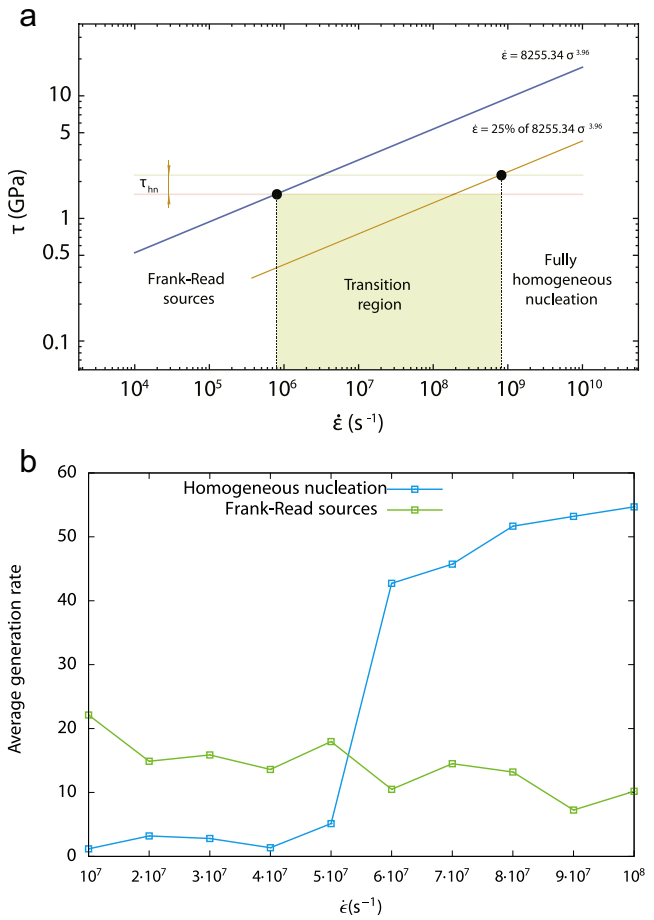

Fig. 14. Dislocation generation by Frank–Read sources and homogeneous nucleation against strain rate. (a) A log–log plot of the peak shear stress τ against strain rate $\dot{\epsilon}$ according to Eq. (34) where $\sigma = 2\tau$. The range of shear stress required to generate dislocations homogeneously is shown by τ_{hn}. In the transition region the contribution to the strain rate effected by homogeneously nucleated dislocations varies between 25% and 100%. At strain rates less than $10^6\ s^{-1}$ Frank–Read sources dominate. At strain rates greater than $10^9\ s^{-1}$ homogeneous nucleation dominates. (b) Average generation rate of dislocations in aluminium by Frank–Read sources and homogeneous nucleation, measured as the number of dislocations generated per time step (1 ps), as a function of strain rate. Computed employing D3P. At strain rates in excess of $6 \times 10^7\ s^{-1}$ homogeneous nucleation becomes the dominant mechanism.

where σ is expressed in GPa and $\dot{\epsilon}$, expressed in s^{-1}, is the strain rate. The shear stress τ on a plane at an angle θ to the shock front is related to σ by the usual stress transformation, $\tau = (\sigma/2)\sin(2\theta)$.

The theoretical lattice strength is typically between $\mu/18$ and $(\pi/4)\mu$ (Meyers et al., 2003). Using Eq. (34) we find that for a theoretical lattice strength of 2.25 GPa ($\approx\mu/8$) strain rates of at least 3×10^6 s^{-1} are required. In Fig. 14a we show the range of strain rates where homogeneous nucleation could supersede Frank–Read sources as the principal mechanism of dislocation generation.

Whether homogeneous nucleation does become the dominant mechanism of dislocation generation at shear stresses above the theoretical strength depends on the activation times of the competing mechanisms. To explore this point we carried out a series of Dynamic Discrete Dislocation Plasticity (D3P) simulations of shock loading at strain rates in the range 10^7–10^8 s^{-1}. D3P is the elastodynamic extension of Discrete Dislocation Plasticity (DDP), a method of discrete dislocation dynamics where plane strain plasticity is studied as the result of the generation and motion of edge discrete dislocations.

4.2.1. Characteristics of the D3P simulation

A rectangular simulation cell was considered of height 0.1 μm normal to the shock direction, and along the shock direction the length was sufficient to accommodate a shock wave. The width δ of the shock wave is given by

$$\delta = \frac{c_l}{\dot{\epsilon}} \cdot \frac{v_0 - v_1}{v_0} \tag{35}$$

where v_0 and v_1 are the unshocked and shocked specific volumes of the material respectively. $\dot{\epsilon}$ is the strain rate of the shock front. v_1 can be found from an equation of state for aluminium such as that in Friedli and Ashcroft (1975). For the range of strain rates considered here $(v_0 - v_1)/v_0 \approx 1$.

The front is made non-advancing, and the rates of generating dislocations homogeneously and from Frank–Read sources are measured. The strain rate was increased in steps of 10^7 s^{-1}. The peak normal stress of the shock wave was computed using Eq. (34). The top and bottom surfaces, parallel to the direction of propagation of the front, were made transparent to dislocations, and the right and left surfaces were made reflective. The isotropic elastic constants of aluminium were employed, with $\mu = 28.3$ GPa, $\nu = 0.36$ and $\rho = 2700$ kg/m^3. The slip planes were assumed to be 0° and $\pm 54.7°$ with respect to the shock axis. The equation of motion of dislocations was assumed to be

$$\frac{d_0 v}{1 - v^2/c_t^2} = \tau b \tag{36}$$

where $d_0 = 2.05 \times 10^{-5}$ Pa s as before.

Frank–Read sources were modelled following the protocols introduced by Gurrutxaga-Lerma et al. (2015a). The dependence of the activation time on the applied stress was obtained from Eq. (26), with $d_0 = 2.05 \times 10^{-5}$ Pa s, and $\tau = (\sigma/2)\sin(2\theta)$. This procedure provided a lower bound on the activation time because a full treatment of the inertial effects would increase the activation time. The source strength was chosen from a log-normal distribution, as described by Shishvan and Van der Giessen (2010), with no offset stress consistent with a pure, single crystal of aluminium. The maximum and minimum Frank–Read source segment lengths were assumed to be $l_{FR}^{\max} = 100$ μm and $l_{FR}^{\min} = 10b$.

As in DDP, the injection equilibrium distance is the minimum separation of two dislocations in the dipole for their mutually attractive forces to be balanced by the applied resolved shear stress. In the elastodynamic case, assuming the dislocations are injected at constant speed v, this can be calculated as follows. The shear stress field of a uniformly moving edge dislocation, with Burgers vector $\mathbf{b} = [b, 0, 0]$, at x and time t on a slip plane at $y = 0$ is given by (vid. Gurrutxaga-Lerma et al., 2013):

$$\sigma_{xy}(x, 0, t) = \frac{b\mu}{\pi s_t^2}\frac{t^2}{x^3}\left[\frac{4\sqrt{1 - x^2/(c_l^2 t^2)}}{(1 - sx/t)}\mathrm{H}(t - x/c_l) - \frac{\left(2 - x^2/(c_t^2 t^2)\right)^2}{(1 - sx/t)\sqrt{1 - x^2/(c_t^2 t^2)}}\mathrm{H}(t - x/c_t)\right] - \sigma_{xy}^{\mathrm{inj}}(x, 0, t) \tag{37}$$

where c_l and c_t are the longitudinal and transverse speeds of sound, $\sigma_{xy}^{\mathrm{inj}}(x, 0, t)$ is the contribution arising from the injection of the dislocations at $t = 0$, H is the Heaviside step function ($\mathrm{H}(t - x/c_t) = 0$ if $t < x/c_t$ and $\mathrm{H}(t - x/c_t) = 1$ if $t > x/c_t$), and $s = 1/v$ is the slowness of the dislocation. Notice that $x = 0$ corresponds to the injection site; the positive x-axis grows in the direction of glide motion of the dislocation.

The injection contribution is given by Gurrutxaga-Lerma et al. (2013)

$$\sigma_{xy}^{\mathrm{inj}}(x, 0, t) = \frac{b\mu}{\pi s_t^2}\frac{t^2}{x^3}\left[\frac{4\left(t^2x^2 - s_l^2x^4\right)}{tx^2\sqrt{t^2 - s_l^2x^2}}\mathrm{H}(t - x/c_l) + \frac{4s_t^2x^4 - 4t^2x^2}{tx^2\sqrt{t^2 - s_t^2x^2}}\mathrm{H}(t - x/c_t) - \frac{s_t^4x^4}{t^3\sqrt{t^2 - s_t^2x^2}}\mathrm{H}(t - x/c_t)\right] \tag{38}$$

where for brevity $s_l = 1/c_l$ and $s_t = 1/c_t$ are the slownesses of sound.

When the equilibrium distance L_{nuc} has been reached, $t = L_{\mathrm{nuc}}/2v = sL_{\mathrm{nuc}}/2$ because the two dislocations are moving with equal speeds in opposite directions along the x-axis. At that instant in time, one dislocation is at position $x = L_{\mathrm{nuc}}/2$, and the other at position $x = -L_{\mathrm{nuc}}/2$ with respect to the injection site. Assuming that the relative speed of a dislocation with respect to another is smaller than the transverse speed of sound (i.e. $2v \le c_t$), then all the Heaviside functions are unity.

In that case, the mobile contribution that one dislocation exerts on the other is

$$\sigma_{xy}^{\text{mobile}}(-L_{\text{nuc}}/2,\,0,\,sL_{\text{nuc}}/2)=4\frac{b\mu}{\pi s_t^2}\frac{s^2}{L_{\text{nuc}}}\left(\frac{\left(2-s_t^2/s^2\right)^2}{4\sqrt{1-s_t^2/s^2}}-\sqrt{1-s_t^2/s^2}\right) \tag{39}$$

and the injection contribution is

$$\sigma_{xy}^{\text{inj}}(-L_{\text{nuc}}/2,\,0,\,sL_{\text{nuc}}/2)=2\frac{b\mu}{\pi s_t^2}\frac{s^2}{L_{\text{nuc}}}\left(-4\left(\sqrt{1-s_l^2/s^2}+\sqrt{1-s_t^2/s^2}\right)-\frac{s_t^4}{s^4\sqrt{1-s_t^2/s^2}}\right) \tag{40}$$

Subtracting the injection contribution from the mobile contribution and equating them to the applied stress τ, the equilibrium distance is obtained

$$L_{\text{nuc}}=\frac{b\mu}{\pi\tau s_t^2}\frac{4s^2\sqrt{s^2-s_l^2}\sqrt{s^2-s_t^2}-s_t^4+4s_t^2s^2-4s^4}{s\sqrt{s^2-s_t^2}} \tag{41}$$

In the event that the relative speed of the dislocations in the dipole is greater than the transverse speed of sound (i.e., $2v>c_t$), then the transverse terms of the fields vanish, and the equilibrium distance takes the form

$$L_{\text{nuc}}=\frac{b\mu}{\pi\tau s_t^2}4s\sqrt{s^2-s_l^2} \tag{42}$$

In the D3P simulations, Frank–Read sources are positioned randomly at the beginning of the simulation, with a source density of 100 μm^{-2}, which is a typical value found in the DDP literature (vid. Balint et al., 2006). Homogeneous nucleation is simulated following the procedures described in Gurrutxaga-Lerma et al. (2014), with a source strength equal to the lattice shear strength of aluminium, taken to be $\tau_{\text{hn}}=2.25$ GPa. Any position in any slip plane is considered a possible site for homogeneous nucleation, provided no other nucleation site is within $10b$ to ensure dipoles do not cross upon injection. The nucleation time is assumed to be smaller than the time step of the simulation, $\Delta t=1$ ps, and dipoles were injected with a random separation distance that follows a Poisson distribution with $\lambda=5b$.

4.2.2. Results and discussion

Upon being loaded, the D3P simulation creates an elastic shock wave which generates dislocations via the two mechanisms. In these simulations the number of dipoles generated per time step by each mechanism is traced, and averaged over $t80$ ps. The results are summarised in Fig. 14b. A well defined transition is shown in the dominant mechanism of dislocation generation from Frank–Read sources at smaller strain rates to homogeneous nucleation at larger strain rates. While there is a fairly steady decline in the contribution of Frank–Read sources throughout the range of strain rates, the increase in the contribution from homogeneous nucleation is abrupt.

Frank–Read source activation: In Section 3, it was shown that the activation time of Frank–Read sources approaches a minimum value asymptotically at strain rates between $10^6\ \text{s}^{-1}$ and $10^8\ \text{s}^{-1}$. This behaviour was traced to the dislocation segments approaching the maximum speed of c_t also asymptotically. The strain rates considered in these simulations, between $10^7\ \text{s}^{-1}$ and $10^8\ \text{s}^{-1}$, are driving the Frank–Read sources at close to their maximum rate of dislocation generation. Consider a Frank–Read source segment of length $4000\sqrt{2}\,b$. The activation time of the segment at $\dot{\epsilon}=10^7\ \text{s}^{-1}$ is about 0.72 ns, following the calculations summarised in Fig. 13. At $\dot{\epsilon}=10^8\ \text{s}^{-1}$ it has decreased to 0.35 ns, close to the minimum activation time of 0.25 ns. At $\dot{\epsilon}=10^7\ \text{s}^{-1}$, the rise time of the shock front is of the order of 10^{-7}s, during which the Frank–Read source generates about 140 dipoles. At $\dot{\epsilon}=10^8\ \text{s}^{-1}$ and rise time of 10^{-8} s, the Frank–Read source generates only about 30 dipoles. In this range of strain rates the rise time of the shock front decreases faster with strain rate than the activation time of Frank–Read sources. If $\dot{\epsilon}$ exceeds $1/(0.25\times10^{-9})=4\times10^9\ \text{s}^{-1}$ these Frank–Read sources are entirely unable to operate before the shock front has passed through.

Homogeneous nucleation: In Fig. 14b a small amount of homogeneous nucleation is evident at strain rates of less than $5\times10^7\ \text{s}^{-1}$. In the D3P simulations, homogeneous nucleation can occur when the resolved shear stress exceeds $\tau_{\text{hn}}=2.25$ GPa. Following the fourth power law (Eq. (34)), the peak normal stress at $10^8\ \text{s}^{-1}$ is 10.85 GPa. At $10^7\ \text{s}^{-1}$, it is 6.03 GPa. The maximum shear stresses on the slip planes are $\tau=5.11$ GPa and $\tau=2.84$ GPa respectively. It follows that throughout the range of strain rates shown in Fig. 14b homogeneous nucleation of dislocations can occur.

At the lower end of the range of strain rates the resolved shear stress is close to τ_{hn}. If the amplitude of the shock front is reduced by the operation of Frank–Read sources the resolved shear stress will be locally insufficient to activate homogeneous nucleation. But as the strain rate increases, and the amount of stress relaxation by Frank–Read sources diminishes, homogeneous nucleation takes over as the dominant mechanism. This is what happens at $\dot{\epsilon}=5\times10^7\ \text{s}^{-1}$. The steep increase in homogeneous nucleation at this strain rate is a consequence of the abundance of available sites for homogeneous nucleation once the stress conditions have been met. The relatively slow increase in the homogeneous generation rate at $\dot{\epsilon}>6\times10^7\ \text{s}^{-1}$ reflects the increased area swept by the front where $\tau>\tau_{\text{hn}}$ as a result of the higher stresses associated with higher strain rates through the fourth power law.

The dominance of homogeneous nucleation when Frank–Read sources are still active is suggestive of a starved system, i.e., the density of Frank–Read sources becomes insufficient to relax the shock front before homogeneous nucleation relaxes it. Our Frank–Read source density of 100 μm^{-2} is a typical value assumed in DDP simulations. There is no reason a priori to choose a different source density in the D3P simulations carried out here. Since homogeneous nucleation can take the generation rate so much above that of Frank–Read sources at these high strain rates the question arises as to whether other generation mechanisms, such as cross-slip (Price, 1963), heterogeneous nucleation at grain boundaries or precipitates, or even twinning may dominate the generation of dislocations at these strain rates. Our D3P simulations support this view because a system capable of only Frank–Read source generation and homogeneous nucleation is starved of dislocations before the homogeneous nucleation can take place. In the presence of the alternative dislocation mechanisms mentioned above, the role of homogeneous nucleation is likely to be diminished, at least in the range of strain rates (10^7–10^8 s^{-1}) shown here.

5. Conclusions

We have examined the finite times required for Frank–Read sources to operate in relation to imposed strain rates ranging from quasistatic to shock loading. In the quasistatic regime, the activation of Frank–Read sources was modelled analytically and by simulations of three dimensional discrete dislocation dynamics (DDD) with the ParaDiS code. At modest strain rates, up to 10^4 s^{-1}, the activation time of Frank–Read sources depends on the inverse of $\dot{\epsilon}$. As the strain rate is increased the shape of the critical configuration of the dislocation segment changes due to the different drag forces acting on edge and screw components for a given dislocation speed. The decrease in the activation time with strain rate is accompanied by an increase in the strength of Frank–Read sources. This leads to an increase of the strain rate sensitivity of the strength of Frank–Read sources which mirrors the increased strain rate sensitivity of the yield point. The strain rate sensitivity, $m = \partial \ln \sigma_{yp} / \partial \ln \dot{\epsilon}$, of the yield stress σ_{yp} of many crystalline metals is approximately 0.01 at strain rates less than 10^4 s^{-1}, but at larger strain rates m increases by about an order of magnitude, with a concomitant steep increase of the yield point. We have shown that the strength of Frank–Read sources displays the same behaviour.

At strain rates greater than $10^6 s^{-1}$, dislocation speeds exceed 1000 m/s in aluminium and both simulations and experiments indicate that the assumption of a drag force proportional to dislocation speed becomes inaccurate. Above this threshold, the increase in the dislocation self-energy with its speed becomes significant. Its speed approaches the transverse speed of sound asymptotically under the influence of an increasing driving stress, as its self-energy increases rapidly. In Section 3 this was taken into account through two distinct models, one where the dislocation was associated with an inertial mass that diverged as the dislocation speed approached c_t, and the other where the drag force diverged in the same limit. These models gave very similar times to activate Frank–Read sources, which was attributed to the fact that both models limit the dislocation speed to c_t.

The existence of a limit to the rate of activation of Frank–Read sources has significant consequences for plastic relaxation at strain rates typical of shock loading. At strain rates of 10^7–10^8 s^{-1} and more models that neglect inertial effects in the dislocation self-energy overestimate the contribution that Frank–Read sources make to plastic relaxation.

Using D3P, an elastodynamic plane strain method of discrete dislocation dynamics, the contributions of Frank–Read sources and homogeneous nucleation were compared. We found that the dominant mechanism of generating dislocations changes abruptly to homogeneous nucleation at strain rates between 5×10^7 s^{-1} and 6×10^7 s^{-1}. However, the contribution of Frank–Read sources declines slowly through this transition, consistent with the inadequacy of Frank–Read sources to relax the shock front at these rates.

Our calculations have shown that D3P is useful for simulating plastic relaxation processes over a range of strain rates encountered in shock loading, enabling us to explore the operation of Frank–Read sources and homogeneous nucleation. The inclusion of dislocation generation by cross-slip in such a plane strain model could be achieved using the 2.5D approach introduced by Benzerga et al. (2004) for D3P's elastostatic counterpart.

Acknowledgements

The authors are grateful to W Cai for providing ParaDiS. B.G.L. acknowledges support by the EPSRC under the EPSRC Doctoral Prize Fellowship scheme.

References

Agnihotri, P.K., Van der Giessen, E., 2015. On the rate sensitivity in discrete dislocation plasticity. Mech. Mater. http://dx.doi.org/10.1016/j.mechmat.2015.01.009, in press.
Argon, A.S., 2008. Strengthening Mechanisms in Crystal Plasticity. Oxford University Press, Oxford, UK.
Armstrong, R.W., Li, Q., 2015. Dislocation mechanics of high-rate deformations. Metall. Mater. Trans. A, 1–16.
Armstrong, R.W., Walley, S.M., 2008. High strain rate properties of metals and alloys. Int. Mater. Rev. 53 (3), 105–128.
Armstrong, R.W., Arnold, W., Zerilli, F.J., 2007. Dislocation mechanics of shock-induced plasticity. Metall. Mater. Trans. A 38, 2605–2610.

Arsenlis, A., Cai, W., Tang, M., Rhee, M., Oppelstrup, T., Hommes, G., Pierce, T.G., Bulatov, V.V., 2007. Enabling strain hardening simulations with dislocation dynamics. Modell. Simul. Mater. Sci. Eng. 15, 553–595.
Aubry, S., Kang, K., Ryu, S., Cai, W., 2011. Energy barrier for homogeneous dislocation nucleation: comparing atomistic and continuum models. Scr. Mater. 64, 1043–1046.
Austin, R.A., McDowell, D.L., 2011. A dislocation-based constitutive model for viscoplastic deformation of fcc metals at very high strain rates. Int. J. Plast. 27 (1), 1–24.
Austin, R.A., McDowell, D.L., 2012. Parameterization of a rate-dependent model of shock-induced plasticity for copper, nickel, and aluminum. Int. J. Plast. 32, 134–154.
Balint, D.S., Deshpande, V.S., Needleman, A., Van der Giessen, E., 2006. Size effects in uniaxial deformation of single and polycrystals: a discrete plasticity analysis. Modell. Simul. Mater. Sci. Eng. 14, 409–442.
Benzerga, A.A., 2008. An analysis of echaustion hardening in micron-scale plasticity. Int. J. Plast. 24, 1128–1157.
Benzerga, A.A., Bréchet, Y., Needleman, A., Van der Giessen, E., 2004. Incorporating three-dimensional mechanisms into two-dimensional dislocation dynamics. Modell. Simul. Mater. Sci. Eng. 12, 159–196.
Bitzek, E., Gumbsch, P., 2004. Atomistic study of drag, surface and inertial effects on edge dislocations in face-centered cubic metals. Mater. Sci. Eng. A 387–389, 11–15.
Bitzek, E., Gumbsch, P., 2005. Dynamic aspects of dislocation motion: atomistic simulations. Mater. Sci. Eng. A 400–401, 40–44.
Bringa, E.M., Caro, A., Wang, Y., Victoria, M., McNaney, J.M., Remington, B.A., Smith, R.F., Torralva, B.R., Van Swygenhoven, H., 2005. Ultrahigh strength in nanocrystalline materials under shock loading. Science 309, 1838–1841.
Bringa, E.M., Rosolankova, K., Rudd, R.E., Remington, B.A., Wark, J.S., Duchaineau, M., Kalantar, D.H., Hawreliak, J., Belak, J., 2006. Shock deformation of face-centred-cubic metals on subnanosecond timescales. Nat. Mater. 5 (10), 805–809.
Brock, L.M., 1982. Dynamic solutions for the non-uniform motion of an edge dislocation. Int. J. Eng. Sci. 20 (1), 113–118.
Brown, L.M., 1964. The self-stress of dislocations and the shape of extended nodes. Philos. Mag. 10 (105), 441–466.
Bulatov, V.V., Cai, W., 2006. Computer Simulations of Dislocation. Oxford University Press, Oxford, UK.
Cai, W., Arsenlis, A., Weinberger, C.R., Bulatov, V.V., 2006. A non-singular continuum theory of dislocations. J. Mech. Phys. Solids 54 (3), 561–587.
Clifton, R.J., Markenscoff, X., 1981. Elastic precursor decay and radiation from nonuniformly moving dislocations. J. Mech. Phys. Solids 29 (3), 227–251.
Crowhurst, J.C., Armstrong, M.R., Knight, K.B., Zaug, J.M., Behymer, E.M., 2011. Invariance of the dissipative action at ultrahigh strain rates above the strong shock threshold. Phys. Rev. B 107, 144302.
Davis, T., Hirth, J.P., 1966. Nucleation rate of vacancy clusters in crystals. J. Appl. Phys. 37 (5), 2112–2116.
Fan, Y., Osetsky, Y.N., Yip, S., Yildiz, B., 2012. Onset mechanism of strain-rate-induced flow stress upturn. Phys. Rev. Lett. 109, 135503.
Follansbee, P.S., Regazzoni, G., Kocks, U.F., 1984. The transition to drag controlled deformation in copper at high strain rates. In: Harding, J. (Ed.), Proceedings of the Third International Conference on Mechanical Properties of Materials at High Strain Rates, vol. 3 of 70. Institute of Physics, London, pp. 71–80.
Foreman, A.J.E., 1967. The bowing of a dislocation segment. Philos. Mag. 15, 1011–1021.
Friedli, C., Ashcroft, N.W., 1975. Aluminum under high pressure. I. Equation of state. Phys. Rev. B 12 (12), 5552–5559.
Gilman, J.J., 1969. Micromechanics of Flow in Solids. McGraw-Hill, New York.
Grady, D.E., 2010. Structured shock waves and the fourth-power law. J. Appl. Phys. 107, 013506.
Gurrutxaga-Lerma, B., Balint, D.S., Dini, D., Eakins, D.E., Sutton, A.P, 2015a. The role of homogeneous nucleation in planar dynamic discrete dislocation plasticity. J.Appl.Mech 82, 071008.
Gurrutxaga-Lerma, B., Balint, D.S., Dini, D., Eakins, D.E., Sutton, A.P., 2013. A dynamic discrete dislocation plasticity method for the simulation of plastic relaxation under shock loading. Proc. R. Soc. A 469, 20130141.
Gurrutxaga-Lerma, B., Balint, D.S., Dini, D., Eakins, D.E., Sutton, A.P., 2014. Dynamic discrete dislocation plasticity. Advances in Applied Mechanics, vol. 47. London, Elsevier (Chapter 2).
Gurrutxaga-Lerma, B., Balint, D.S., Dini, D., Eakins, D.E., Sutton, A.P., 2015b. Attenuation of the dynamic yield point of shocked aluminum using elasto-dynamic simulations of dislocation dynamics. Phys. Rev. Lett. 114, 174301, http://dx.doi.org/10.1103/PhysRevLett.114.174301.
Gutkin, M.Y., Ovidko, I.A., 2006. Special mechanism for dislocation nucleation in nanomaterials. Appl. Phys. Lett. 88, 211901.
Gutkin, M.Y., Ovidko, I.A., 2008. Homogeneous nucleation of dislocation loops in nanocrystalline metals and ceramics. Acta Mater. 56, 1642–1649.
Hirth, J.P., Lothe, J., 1982. Theory of Dislocations, 2nd ed. John Wiley & Sons, New York.
Hirth, J.P., Zbib, H.M., Lothe, J., 1998. Forces on high velocity dislocations. Modell. Simul. Mater. Sci. Eng. 6, 165–169.
Huang, J.C., Gray III, G.T., 1989. Microband formation in shock-loaded and quasi-statically deformed metals. Acta Metall. 37 (12), 3335–3347.
Hull, D., Bacon, D.J., 2011. Introduction to Dislocations, 5th ed. Butterworth-Heinemann, Oxford, UK.
Iserles, A., 2009. A First Course in the Numerical Analysis of Differential Equations, vol. 44. Cambridge University Press, Cambridge, UK.
Johnston, W.G., Gilman, J.J., 1959. Dislocation velocities, dislocation densities, and plastic flow in lithium fluoride crystals. J. Appl. Phys. 30 (2), 129–144.
Klopp, R.W., Clifton, R.J., Shawki, T.G., 1985. Pressure-shear impact and the dynamic viscoplastic response of metals. Mech. Mater. 4 (3), 375–385.
Koizumi, H., Kirchner, H.O.K., Suzuki, T., 2002. Lattice wave emission from a moving dislocation. Phys. Rev. B 65, 214104.
Lloyd, J.T., Clayton, J.D., Becker, R., McDowell, D.L., 2014. Simulation of shock wave propagation in single crystal and polycrystalline aluminum. Int. J. Plast. 60, 118–144.
Malygin, G.A., Ogarkov, S.L., Andriyash, A.V., 2013. On the power-law pressure dependence of the plastic strain rate of crystals under intense shock wave loading. Phys. Solid State 55 (4), 780–786.
Markenscoff, X., 1980. The transient motion of a nonuniformly moving dislocation. J. Elast. 10 (2), 193–201.
Markenscoff, X., Clifton, R.J., 1981. The nonuniformly moving edge dislocation. J. Mech. Phys. Solids 29 (2), 253–262.
Meyers, M.A., 1978. A mechanism for dislocation generation in shock-wave deformation. Scr. Metall. 12, 21–26.
Meyers, M.A., 1994. Dynamic Behavior of Materials. John Wiley, Hoboken, NJ.
Meyers, M.A., Gregori, F., Kad, B.K., Schneider, M.S., Kalantar, D.H., Remington, B.A., Ravichandran, G., Boehly, T., Wark, J.S., 2003. Laser-induced shock compression of monocrystalline copper: characterization and analysis. Acta Mater. 51, 1211–1228.
Meyers, M.A., Jarmakani, H., Bringa, E.M., Remington, B.A., 2009. Dislocations in shock compression and release. In: Hirth, J.P., Kubin, L.P. (Eds.), Dislocations in Solids, vol. 15. North-Holland, Amsterdam, pp. 94–197. (Chapter 89).
Murr, L.E., 1988. Shock Waves in Condensed Matter-1988. Elsevier, Amsterdam315.
Murr, L.E., Kuhlmann-Wilsdorf, D., 1978. Experimental and theoretical observations on the relationship between dislocation cell size, dislocation density, residual hardness, peak pressure and pulse duration in shock-loaded nickel. Acta Metall. 26 (5), 847–857.
Ni, L., Markenscoff, X., 2008. The self-force and effective mass of a generally accelerating dislocation I: screw dislocation. J. Mech. Phys. Solids 56 (4), 1348–1379.
Nix, W.D., Menezes, R.A., 1971. Physics of strengthening mechanics in crystalline solids. Annu. Rev. Mater. Sci. 1, 313–346.
Olmsted, D.L., Hector, L.G., Curtin, W.A., Clifton, R.J., 2005. Atomistic simulations of dislocation mobility in Al, Ni and Al/Mg alloys. Modell. Simul. Mater. Sci. Eng. 13, 371–388.
Pellegrini, Y.-P., 2014. Equation of motion and subsonic-transonic transitions of rectilinear edge dislocations: a collective-variable approach. Phys. Rev. B 90 (5), 054120.
Pillon, L., Denoual, C., Pellegrini, Y.-P., 2007. Equation of motion for dislocations with inertial effects. Phys. Rev. B 76 (22), 224105.
Price, P.B., 1963. Direct Observations of Glide, Climb, and Twinning in Hexagonal Metal Crystals. Wiley-Interscience, New York41–129.
Reed-Hill, R.E., Abbaschian, R., Abaschian, L., 2009. Physical Metallurgy Principles, 4th ed. Cengage Learning, Stamford, CT.
Regazzoni, G., Kocks, U.F., Follansbee, P.S., 1987. Dislocation kinetics at high strain rates. Acta Metall. 35 (12), 2865–2875.

Shishvan, S.S., Van der Giessen, E., 2010. Distribution of dislocation source length and the size dependent yield strength in freestanding thin films. J. Mech. Phys. Solids 58 (5), 678–685.
Shishvan, S.S., Mohammadi, S., Rahimian, M., 2008. A dislocation-dynamics-based derivation of the Frank–Read source characteristics for discrete dislocation plasticity. Modell. Simul. Mater. Sci. Eng. 16, 075002.
Swegle, J.W., Grady, D.E., 1985. Shock viscosity and the prediction of shock wave rise times. J. Appl. Phys. 58 (2), 692–701.
Taylor, J.W., 1969. Hypervelocity Impact Phenomena. Academic Press, New York.
Tschopp, M.A., McDowell, D.L., 2008. Influence of single crystal orientation on homogeneous dislocation nucleation under uniaxial loading. J. Mech. Phys. Solids 56, 1806–1830.
Tsuzuki, H., Branicio, P.S., Rino, J.P., 2008. Accelerating dislocations to transonic and supersonic speeds in anisotropic metals. Appl. Phys. Lett. 92, 191909.
Van der Giessen, E., Needleman, A., 1995. Discrete dislocation plasticity: a simple planar model. Modell. Simul. Mater. Sci. Eng. 3 (5), 689–735.
Wang, Z.Q., Beyerlein, I., LeSar, R., 2007. The importance of cross-slip in high-rate deformation. Modell. Simul. Mater. Sci. Eng. 15 (6), 675.
Weertman, J., 1961. High velocity dislocations. In: Shewmon, P.G., Zackay, V.F. (Eds.), Response of Metals to High Velocity Deformation. Metallurgical Society Conferences, vol. 9. Metallurgical Society of AIME. Interscience, New York, pp. 205–249.
Weertman, J., 1986. Plastic deformation behind strong shock waves. Mech. Mater. 5, 13–28.
Weertman, J., Follansbee, P.S., 1988. Dislocation dynamics and plastic shock waves. Mech. Mater. 7, 177–189.
Weertman, J., Weertman, J.R., 1980. Moving dislocations. In: Nabarro, F.R.N. (Ed.), Dislocations in Solids, vol. 3. North-Holland, Amsterdam, pp. 3–59. (Chapter 8).
Zaretsky, E., 1995. Dislocation multiplication behind the shock front. J. Appl. Phys. 78 (6), 3740–3747.